# Electrochemical Reaction and Dissociation of Glycerol on PdAu Surface Catalyst
(Tindak Balas Elektrokimia dan Pemisahan Gliserol pada Permukaan Pemangkin PdAu)

Nabila A. Karim*, Norilhamiah Yahya, Muhammad Syafiq & Siti Kartom Kamarudin

ABSTRACT

*Direct Glycerol Fuel Cell is one of the alternative energy that can produce electricity without burning. The production of electricity without combustion can reduce the use of fossil fuel as well as reduce environmental pollution. A new catalyst of PdAu has been synthesized in this study to increase the activity of the glycerol oxidation reaction. Morphologies analysis was performed on CNF-supported synthesized PdAu. FESEM and TEM image show the PdAu supported on the CNF surface. Both PdAu and CNF has a diameter size of 4-6 nm and 80-130 nm, respectively. In CV analysis, PdAu/CNF has produced an oxidation peak and current density at -0.9 V vs. SCE and 70 mA/cm², respectively. Each mechanism of glycerol dissociation step during glycerol oxidation, different atomic active sites are required in PdAu. For example, for glycerol adsorption, Au atom as an active site while for \*$C_3H_7O_3$ requires Pd atom and Au atom as the active site. The Au catalyst model shows better adsorption as Au/CNF has a slightly more negative oxidation peak than PdAu. Nevertheless, the Au catalyst showed less durability compared to PdAu.*

Keywords: Electro-catalyst; electrochemical reaction; glycerol; PdAu; surface reaction

ABSTRAK

*Sel Bahan Api Gliserol Langsung adalah salah satu tenaga alternatif yang dapat menghasilkan elektrik tanpa proses pembakaran. Pengeluaran elektrik tanpa pembakaran dapat mengurangkan penggunaan bahan bakar fosil serta mengurangkan pencemaran alam sekitar. Mangkin baru PdAu telah disintesis dalam kajian ini untuk meningkatkan aktiviti tindak balas pengoksidaan gliserol. Analisis morfologi dilakukan pada PdAu yang telah disintesis dan disokong oleh CNF. Gambar FESEM dan TEM menunjukkan PdAu disokong pada permukaan CNF. Kedua-dua PdAu dan CNF masing-masing mempunyai ukuran diameter 4-6 nm dan 80-130 nm. Dalam analisis CV, PdAu/CNF telah menghasilkan puncak pengoksidaan dan ketumpatan arus masing-masing pada -0.9 V vs SCE dan 70 mA/cm². Setiap mekanisme langkah pemisahan gliserol semasa pengoksidaan gliserol, tapak aktif atom yang berbeza diperlukan dalam PdAu. Sebagai contoh, untuk penjerapan gliserol, atom Au sebagai tapak aktif sementara untuk \*$C_3H_7O_3$ memerlukan atom Pd dan atom Au sebagai tapak aktif. Model mangkin Au menunjukkan penjerapan yang lebih baik kerana Au/CNF mempunyai puncak pengoksidaan yang sedikit lebih negatif daripada PdAu. Walaupun begitu, mangkin Au menunjukkan daya tahan yang lebih rendah berbanding dengan PdAu.*

Kata kunci: Elektro-mangkin; gliserol; permukaan tindak balas; PdAu tindak balas elektrokimia

## INTRODUCTION

The use of fossil fuel in energy production has caused fossil fuel resources to decrease and also cause environmental pollution (Alias et al. 2020; Day & Day 2017; Wang et al. 2018). Therefore, alternative energy is needed to replace the use of fossil fuel. Various alternative energy is being developed, and fuel cells have shown one of the technologies to be proud of to replace fossil fuel (Wang et al. 2018). Fuel cells have different types depending on fuel consumption (Karim & Kamarudin 2017). Polymer electrolyte membrane fuel cell uses hydrogen as fuel. The use of hydrogen as fuel despite producing high energy, but problems such as storage and transportation have led to the use of Direct Liquid Fuel Cell (DLFC) (Abdullah et al. 2017; Mori & Hirose 2009).

Glycerol is one of the forms in DLFC and is called Direct Glycerol Fuel Cell (DGFC). The use of glycerol as fuel has advantages such as low pollution, high energy density, rapid start-up, simplicity, and few safety concerns (Karim et al. 2017). Glycerol has a more complex structure compared to methanol leading to the production of various intermediate reactions (Yahya et al. 2017). The complex structure also leads to a sluggish reaction in the DGFC (Nascimento & Linares 2014; Zakaria et al. 2019).

Commonly used catalysts in the glycerol oxidation reaction are Pt and Pt-based catalysts (Wang et al. 2017). Tam et al. (2019) synthesized the PtRu to enhance the electrochemical reaction of glycerol compared to bare Pt. The authors found that there are about 40% of Pt (100) sites and only a small amount of Pt (111) sites. A different facet of the Pt gives different catalytic activity and mechanism reactions of glycerol. The addition of Ru metal in Pt to form PtRu alloy showed an increase in the onset potential for the oxidation of carbon monoxide (CO). The CO is the last intermediate product before a complete glycerol oxidation reaction. A study by Brueckner et al. (2019) used Sn oxide as support for the PtRu and PtRh catalyst. The PtRu catalyst showed remarkable catalytic activity of the glycerol oxidation compared to the PtRh. The authors also stated that these catalysts are not as highly active as compared using other fuels such as methanol and ethanol.

Martins et al. (2019) investigated the *in-situ* preparation of PtFe/C to prevent the costly and time-consuming preparation of catalysts for the oxidation reaction of glycerol (Martins et al. 2019). The *in-situ* technique can control and increase the Fe ad-atom on the Pt metal. The ultra-low loading of Fe in PtFe has increased the power density by 36%, reaching 54 mW/cm$^2$. Zhou et al. (2019) synthesized the PtAg skeleton showed 15.4 times higher in activity compared to the Pt/C. The authors also conducted the product analysis using liquid chromatography and found that the product of dihydroxyacetone showed 82.6% selectivity in the glycerol oxidation reaction. Other product compounds found in the same analysis are tartronic acid, glyceric acid, glyceraldehyde, glycolic acid, oxalate acid, and glyoxylic acid.

Gao et al. (2019) synthesized the 1D structure of PtNi for the high catalytic activity of the glycerol oxidation reaction. Different structures of PtNi have been developed in this study, and there are ultrafine nanowires, sinuous nanowires, and ultrashort nanowires. The structures obtained by controlling the amount of citric acid, ascorbic acid, and glucose. The electrochemical reaction and mass activity increase about 4.3 and 3.9 times higher than the commercial catalyst of Pt/C, respectively. Zhang et al. (2019) also conducted the PtNi nanorod and found the optimized atomic ratio Pt to Ni is the best at 3:1 for the glycerol oxidation reaction. The value of the mass activity is 4601.5 mA/mg, which is 4.6 times higher than commercial Pt/C.

While Araujo et al. (2019) studied the effect of Sn adsorption on the Pt surface for the electrochemical oxidation reaction of glycerol, the authors found that there are sequences in the facet of adsorption of Sn on Pt that increase the activity of glycerol oxidation reaction. The sequence facet that has high activity is (100) terraces followed by the (100) short domains and then the (110) domains. However, the oxidation of CO is low on (100) terraces. Not only that, the addition of Sn on the Pt surface also increases the breaking bond of C-C in glycerol. Sun et al. (2019) studied the different atomic ratio of Pt and Co in PtCo nanowires for the electrochemical oxidation reaction of glycerol. The PtCo that has an atomic ratio 89:11 is the best ratio for glycerol oxidation reaction give mass and specific activities of 4573.0 mA/mg and 11.9 mA/cm$^2$, respectively. In addition to the attractive catalyst structure and high catalytic surface area, the use of support also plays an important role in increasing the electrochemical reaction activity of the glycerol. Various catalyst support has been produced, such as graphene foam (Cui et al. 2019), carbon nanotubes (Ning et al. 2019), and graphitic carbon nanosheets (Ghosh et al. 2019). Cui et al. (2019) used the graphene foam as support for ultra-small Pd nanoparticles. The graphene foam is synthesized from lamellar MCM-22 zeolite as a template has given the catalytic activity as 1.7-2.9 times higher than the Pd/C commercial catalyst. A carbon nanotube that has been doped with S to support the Pt nanoparticle catalyst was produced by Ning et al. (2019). The interaction of carbon and sulphur atoms in the S-doped carbon nanotubes has reduced the formation of poisonous intermediates and in thus, has increased catalyst stability.

The use of the Pt catalyst prone to be poisoned and costly (Karim et al. 2017). Therefore, the search for catalyst production other than Pt is very necessary. Pd catalyst has advantages and durability compared to Pt-based catalyst (Wang et al. 2017). Houache et al. (2019) developed the NiPd alloy for electro-oxidation of glycerol, and they found that formation of various by-products using polarization modulation infrared reflection absorption spectroscopy analysis. The primary by-products are mesoxalate, tartronate, and glyceraldehyde.

A study by Ghosh et al. (2019) that using PdFe as a catalyst in various atomic ratios of Pd to Fe. The authors found that the mass activity of the glycerol is 1.86 A/mg is higher using PdFe compared to the PdPt nanowires and other Pd-based catalysts. At the same time, Wang et al. (2019) investigated the effect of PdAg particle size towards the glycerol electro-oxidation reaction. The authors synthesized several particle sizes from 3.1 to 7.8 nm. The PdAg that have a particle size of 3.1 nm showed remarkable and excellent activity with the mass activity of 3.51 A/mg compared to other PdAg particle sizes. The addition of other metals to form alloy in pure Pd is beneficial because it can reduce agglomeration in pure Pd metal. Metal Au was selected in this study because of Au's resistance in a harsh environment. In addition, there is no study that investigate how the glycerol is dissociate at the catalyst surface during the glycerol oxidation reaction. Therefore, this study has been conducted

in both experimental and theoretical studies for the electrochemical oxidation reaction and dissociation of glycerol using PdAu as a catalyst.

## MATERIALS AND METHODS

All the reagent was bought from the Sigma-Aldrich. The 0.05 M $PdCl_2$ (in 0.1 M HCl) was mixed with 0.05 M of $AuCl_3 \cdot HCl \cdot 4H_2O$ bring a total solution of 15 mL. Some amount of trisodium citrate was dropped wisely. Then, this solution was added drop-wise to a stirred CNF slurry (isopropanol and deionized water) and went for 2 h. After that, the reduction of the metal precursors is carried out using an appropriate amount of freshly prepared ice-cold sodium borohydride ($NaBH_4$), and the solution was stirred overnight at 10 ºC. Longer reaction time is needed to allow the sodium borohydride as it has strong reducing abilities to react with metal precursors to form the catalyst. The molar ratio $NaBH_4$: metal ions were taken at 5:1. The final product was filtered and washed with deionized water several times and dried at 80 ºC overnight. The synthesized catalysts are further morphological analysis using x-ray diffraction (XRD), field emission scanning electron microscope (FESEM), and transmission electron microscopy (TEM).

The cyclic voltammetry measurement was performed by using Autolab electrochemical workstation at room temperature. The catalyst ink solution was carefully deposited onto the glassy carbon electrode surface by using a micropipette. The deposited catalyst was leave dried at room temperature. The electrochemical characterization of catalyst samples was studied in the potential range -0.7 to 0.4 V in 50 mV/s in 1 M KOH and at scan rate 50 mV/s in 0.5 M glycerol/1 M KOH solution. Both solutions were deoxygenated by bubbling with $N_2$ at 200 mL/min for 30 min before taking any measurement of the glycerol oxidation reaction.

The Materials Studio DMol3 (Version 5.5) is used in this study. Density functional theory (DFT) calculations were carried out with the PBE functional, while the effective potential with relativistic effect-accounted DFT semi-core DSPP was used for all calculations. DNPs, double numerical plus polarization function basis sets, was employed for all the calculations. The Monkhorst-Pack grid was set to 3×3×1. The spin unrestricted method was used for all open-shell systems. The SCF criterion used was $1\times10^{-5}$ Hartree for the total energy. All structures were fully optimized without any symmetry constraints, with a convergence criterion of 0.004 Ha Å$^{-1}$ for the forces, 0.005 Å for the displacement, and $2\times10^{-5}$ Ha for the energy change. Negative adsorption energy indicates that the adsorption is stable (exothermic) with respect to the free gas phase adsorbate.

## RESULTS AND DISCUSSION

### MORPHOLOGY OF THE PDAU CATALYST SUPPORTED ON CNF

Figure 1 shows the FESEM image of the PdAu catalyst supported on the CNF. As seen from the figure, the long rod refers to the CNF support materials. It looks very clear, showing that the small spherical particles are on the surface of the PdAu catalyst. These small spherical particles, refer to the nanoparticle of PdAu, have been supported by CNF. Figure 2 shows the TEM image of
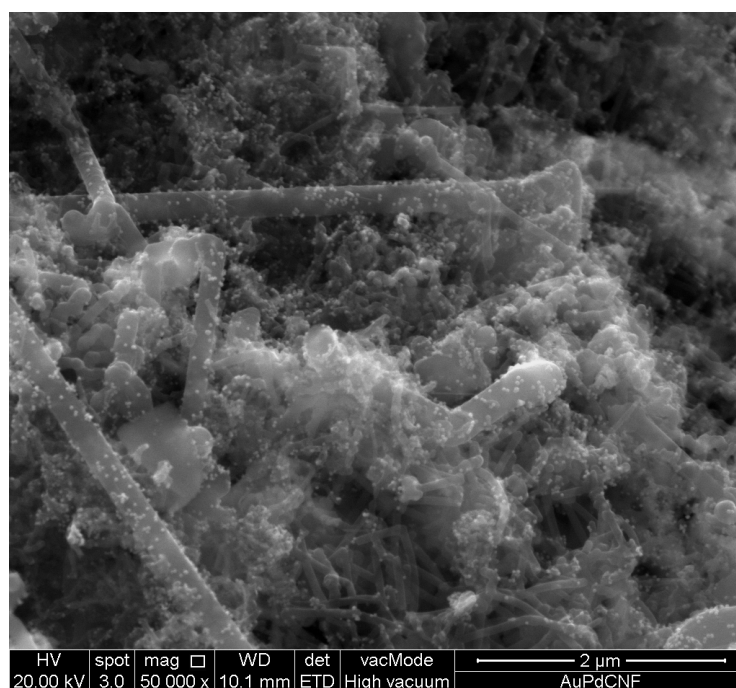


FIGURE 1. The FESEM image of the PdAu supported on CNF

the PdAu supported on CNF. From Figure 2, the CNF has an average diameter size of 80 to 130 nm. The small particles located on the CNF surface refer to PdAu nanoparticles having an average diameter size of 4 nm to 6 nm. There is also a slight agglomeration of PdAu on the CNF surface. The synthesis of Pd alone is very difficult because Pd tends to agglomerate (Zhang et al. 1993). Pd alloyed with other metals can reduce agglomeration. Overall, PdAu synthesized and supported by CNF has successfully reduced the agglomeration of nanoparticles.

Figure 3 shows the XRD pattern for the Au/CNF, Pd/CNF, and PdAu/CNF. The Au/CNF and Pd/CNF are also analyzed in the XRD pattern as references. From Figure 3, Au/CNF has diffraction peaks at 38.08, 44.21, 65.01, and 77.80° correspond to the (111), (200), (220), and (311), respectively. While the Pd/CNF has the diffraction peaks at 39.84, 46.53, 67.53, and 81.61° refer to the (111), (200), (220), and (311), respectively. However, there is an apparent change in position of the diffraction peaks from the Pd/CNF position towards the Au/CNF position.
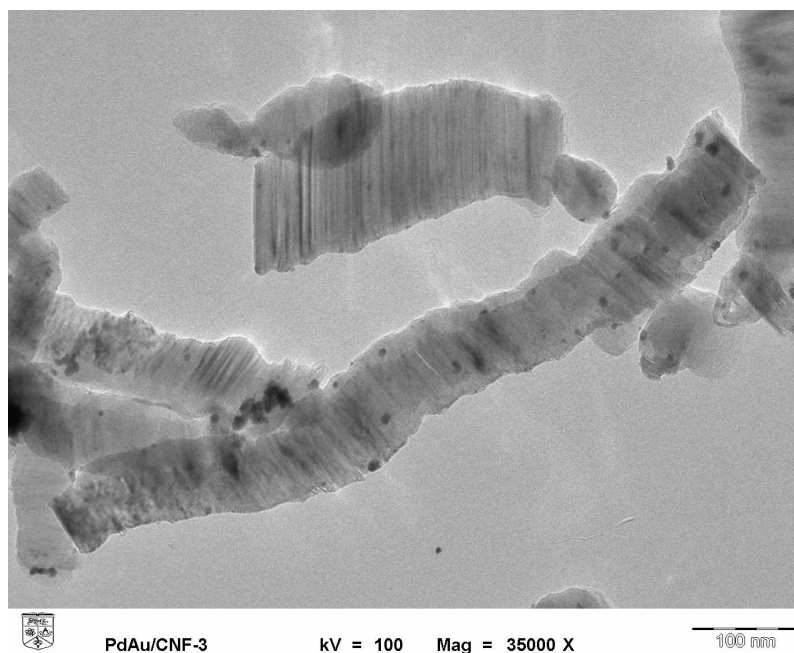


PdAu/CNF-3          kV = 100     Mag = 35000 X          100 nm

FIGURE 2. The TEM image of the PdAu supported on CNF
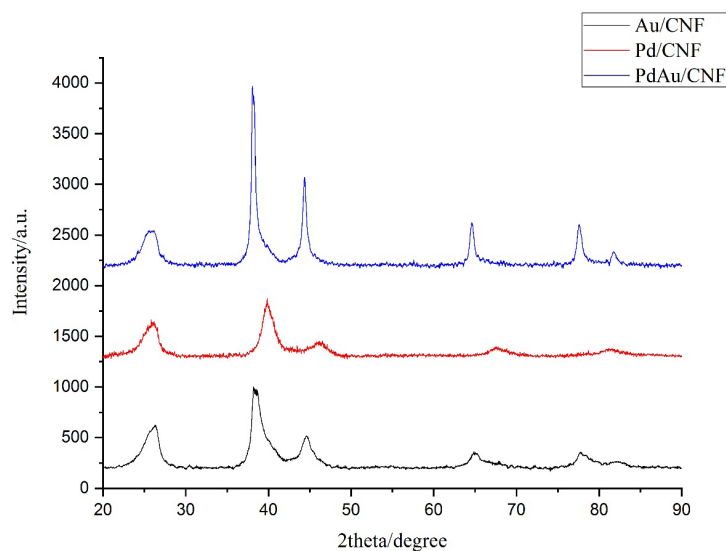


FIGURE 3. XRD pattern of the catalyst samples, Au/CNF, Pd/CNF, and PdAu/CNF

## ELECTROCHEMICAL REACTION OF THE PDAU IN GLYCEROL

Figure 4 shows the cyclic voltammetry test in 50 mV/s in 1 M KOH for Au/CNF, Pd/CNF, and PdAu/CNF. There is no clear peak of Au/CNF tested in this solution. However, the Pd/CNF has a reduction peak occur at -0.38 V vs. SCE, and alloying the Pd with the Au in PdAu/CNF showed a shifted peak at -0.4 V vs. SCE. The catalysts are further tested in 50 mV/s in 0.5 M glycerol/1 M KOH solution, as shown in Figure 5. From Figure 5, the Au/CNF shows the lowest current density during the glycerol electrochemical reaction of 45 mA/cm². The oxidation peak of glycerol using Au/CNF is at -0.1 V vs. SCE. Compared to Pd/CNF has a more negative oxidation peak at -0.12 V vs. SCE. The current density at the oxidation peak in Pd/CNF is also higher than Au/CNF, which is 50 mA/cm². When inserting Au metal in Pd into PdAu and supported by CNF, the oxidation peak of the glycerol shifted a little positive at -0.09 V vs. SCE. However, the current density at glycerol oxidation peak using PdAu/CNF showed a very significant increase to 70 mA/cm². CNF-supported PdAu alloys have increased glycerol oxidation activity compared to Pd/CNF and Au/CNF.
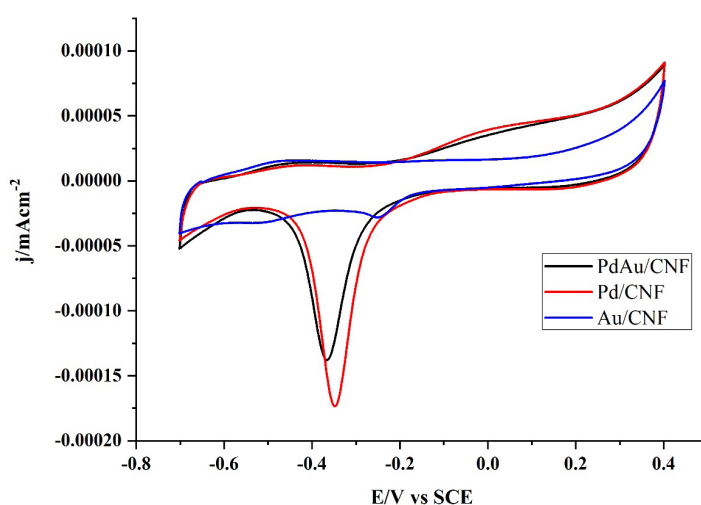


FIGURE 4. Cyclic voltammetry (CV) test in 50 mV/s in 1 M KOH for different catalyst samples
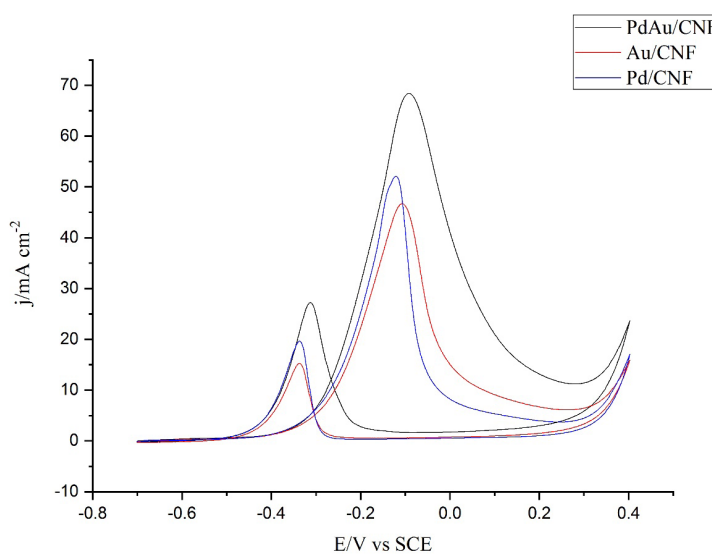


FIGURE 5. Cyclic voltammetry (CV) test in 50 mV/s in 0.5 M glycerol/1 M KOH solution for different catalyst samples

ADSORPTION PROPERTIES AND DISSOCIATION OF THE
GLYCEROL ON PDAU ALLOY SURFACE

PdAu alloy catalyst is further studied from the theoretical surface reaction point using density functional theory (DFT). Using this technique, glycerol dissociation during the oxidation reaction of glycerol can be studied. The adsorption energy on the dehydrogenation of glycerol is calculated as:

$$\Delta E = E_{C_3H_xO_3^*} - E_* - E_{glycerol(g)} + \frac{8-x}{2}E_{H_2(g)} \quad (1)$$

Tables 1 and 2 show the properties of adsorption species that occur on the catalyst surfaces of PdAu and Au, respectively. Au catalyst surface model was used as a comparison with PdAu in this study. The reaction mechanism of the glycerol dissociation is from (2) to (8).
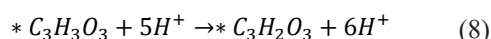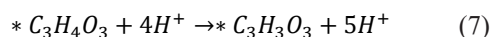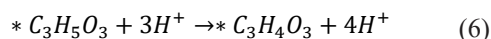
$$C_3H_8O_3 \rightarrow * C_3H_8O_3 \quad (2)$$

$$* C_3H_8O_3 \rightarrow * C_3H_7O_3 + H^+ \quad (3)$$

$$* C_3H_7O_3 + H^+ \rightarrow * C_3H_6O_3 + 2H^+ \quad (4)$$

$$* C_3H_6O_3 + 2H^+ \rightarrow * C_3H_5O_3 + 3H^+ \quad (5)$$

$$* C_3H_5O_3 + 3H^+ \rightarrow * C_3H_4O_3 + 4H^+ \quad (6)$$

$$* C_3H_4O_3 + 4H^+ \rightarrow * C_3H_3O_3 + 5H^+ \quad (7)$$

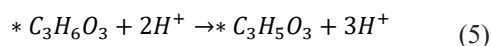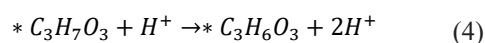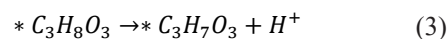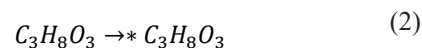$$* C_3H_3O_3 + 5H^+ \rightarrow * C_3H_2O_3 + 6H^+ \quad (8)$$

TABLE 1. Adsorption properties of the species adsorbate on the PdAu catalyst surface

| Adsorbate | Adsorption energy, Eads (eV) | Bond length Au-O (Å) | Bond length Pd – O (Å) | Bond length Au – C (Å) | Bond length Pd – C (Å) |
|---|---|---|---|---|---|
| CH$_2$OHCHOHCH$_2$OH | -0.34 | 2.87 | - | - | - |
| CHOH$_2$COHCH$_2$OH | 0.46 | - | 3.56 | 3.81 | - |
| CH$_2$OHCOCH$_2$OH | 0.47 | - | 3.80 | - | - |
| CHOHCOCH$_2$OH | 1.32 | - | 3.35 | - | 4.03 |
| CHOHCOCHOH | 1.70 | - | - | 3.73 | 3.15 |
| CHOHCOCHO | 2.00 | - | 2.14 / 2.23 | - | |
| CHOCOCHO | 2.96 | 3.11 | 2.09 / 2.27 | - | - |
| CHOCO | -13.87 | - | - | - | 2.00 |
| CO | 0.61 | - | - | - | 1.91 |

TABLE 2. Adsorption properties of the species adsorbate on the Au catalyst surface

| Adsorbate | Adsorption energy, Eads (eV) | Bond length Au-O (Å) | Bond length Au – C (Å) |
|---|---|---|---|
| CH$_2$OHCHOHCH$_2$OH | -0.76 | 2.85 / 3.25 | - |
| CHOH$_2$COHCH$_2$OH | -0.01 | 3.47 | 3.67 |
| CH$_2$OHCOCH$_2$OH | -0.03 | 3.74 | - |
| CHOHCOCH$_2$OH | 1.05 | 4.07 | 3.93 |
| CHOHCOCHOH | 1.22 | - | 3.26 / 3.72 |
| CHOHCOCHO | 1.97 | 2.30 / 2.47 | - |
| CHOCOCHO | 2.96 | 2.81 / 2.36 / 2.96 | - |
| CHOCO | -13.92 | | 2.13 |
| CO | 1.01 | | 2.05 |

The mechanism of the dehydrogenation to produce proton in the electrochemical reaction started as the glycerol is adsorbed on the PdAu surface, as shown in Figure 6(a) and (2). All the adsorption positions in this paper have been optimized. In Figure 6(a), the glycerol is adsorbed on the Au atom in PdAu through oxygen atom in glycerol. This adsorption generates the adsorption energy of -0.34 eV, as shown in Table 1. The bond length of the Au atom and oxygen atom after the adsorption occurs is 2.87 Å.
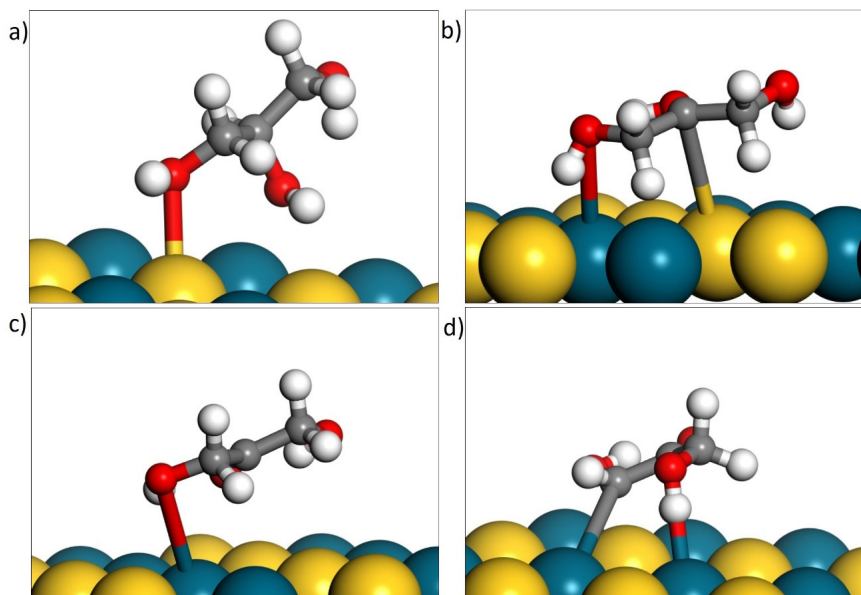


FIGURE 6. Adsorption species on PdAu catalyst surface (a) glycerol or $CH_2OHCHOHCH_2OH$, (b) $CHOH_2COHCH_2OH$, (c) $CH_2OHCOCH_2OH$ and (d) $CHOHCOCH_2OH$

Next for dehydrogenation reaction or next hydrogen dissociation from the glycerol occur as in reaction (3) which produces adsorbate $*C_3H_7O_3$ and a proton. Figure 6(b) shows how this adsorbate is adsorbed on the surface of PdAu, i.e., through oxygen atom is adsorbed on Pd atom (Pd-O), and the carbon atom in $*C_3H_7O_3$ is adsorbed on Au atom (Au-C) in PdAu. Both bond lengths of Pd-O and Au-O are 3.56 Å and 3.81 Å, respectively. This adsorption has produced an adsorption energy of 0.46 eV.

The next hydrogen dissociation from the glycerol to produce adsorbate of $*C_3H_6O_3$ as (4) has adsorbed on the surface of PdAu through Pd atoms. Through this, adsorption has produced an adsorption energy of 0.47 eV. The bond length of Pd-O elongated to 3.80 Å compared to adsorption through (3). Subsequent adsorption produces an adsorbate of $*C_3H_5O_3$ in (5) as shown in Figure 6(d). This adsorption requires two active sites Pd atoms have produced adsorption energy of 1.32 eV. Both Pd-O and Pd-C have produced bond lengths of 3.35 Å and 4.03 Å, respectively.
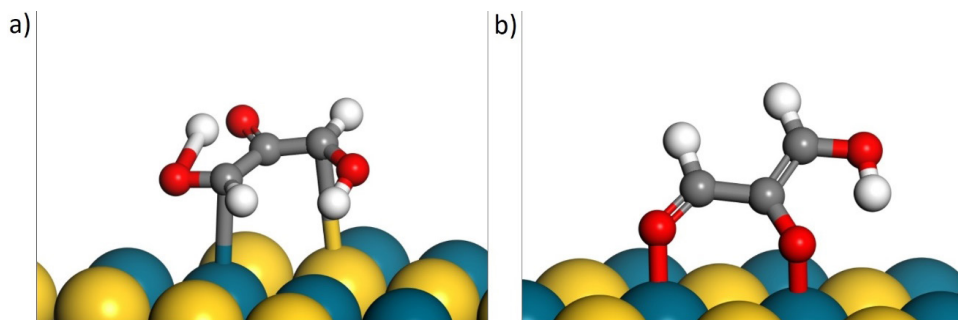


FIGURE 7. Adsorption species on PdAu catalyst surface (a) CHOHCOCHOH and (b) CHOHCOCHO

Each mechanism step in glycerol oxidation requires a different active site. Such as the next dissociation in (6) which produces adsorbate of $*C_3H_4O_3$ requires Pd and Au active site for both carbons in $*C_3H_4O_3$ to be adsorbed. Figure 7(a) shows which carbon atoms in the adsorbate of $*C_3H_4O_3$ have adsorbed on the surface of PdAu with adsorption energy of 1.70 eV. This adsorption has resulted in a bond length of Pd-C and Au-C of 3.15 and 3.73 Å, respectively. Further dissociation in (7) has produced by position adsorbate atoms on both Pd atoms, as shown in Figure 7(b). Both bonding at these Pd atoms is 2.09 Å and 2.23 Å with an adsorption energy of 2.00 eV. Further dissociation on the surface of PdAu has produced $*C_3H_2O_3$ adsorbate, as shown in (8) and Figure 8(a). In Figure 8(a), three atom oxygens in $*C_3H_2O_3$ adsorbed on two Pd atoms and an Au atom. These three bonding (two Pd-O and one Au-O) have value, as shown in Table 1 is 2.09, 2.27, and 3.11 Å, respectively.
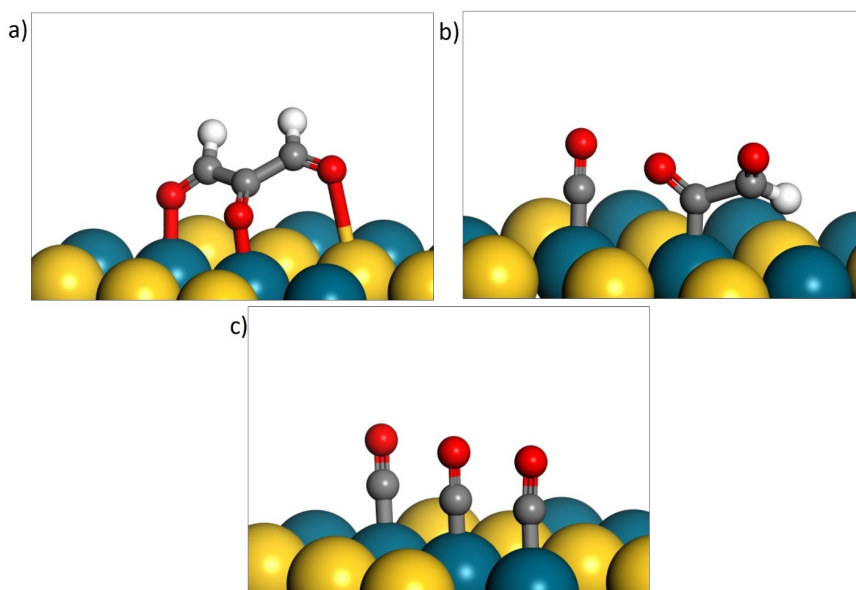


FIGURE 8. Adsorption species on PdAu catalyst surface (a) CHOCOCHO, (b) CHOCO and CO and (c) three molecules of CO

The adsorbate $*C_3H_2O_3$ is breaking to form $*COCOH$ and $*CO$ adsorbate on PdAu, as shown in (9) and Figure 8(b). The optimized model shows that this adsorbate is more stable in adsorption on Pd atoms than Au atoms. Adsorption energy generated through this adsorption for (9) is -13.87 eV. The bond length Pd-C in $*COCOH$ has been produced with a value of 2.27 Å. While Pd-C in $*CO$ has produced a bong length of 2.09 Å. The $*COCOH$ adsorbate then dissociates to form three $*CO$ molecules on the surface of PdAu, as shown in (10) and Figure 8(b). A weak adsorption energy value of 0.61 eV has been produced with a bond length of Pd-C is 1.91 Å.

From the experiment section in CV analysis, Au/CNF showed a slightly better oxidation peak, which is a little more negative than PdAu. If we look at the comparison from a theoretical point of view, namely the dissociation of glycerol PdAu and Au, as shown in Tables 1 and 2, the Au model also shows a slightly better dissociation than PdAu. Both theoretical and experimental results support each other. However, PdAu/CNF has a higher current density than Pd/CNF and Au/CNF because it is supported by CNF. In addition, the theoretical result has showed something where experimental cannot be tested, namely the final step of CO adsorption.

The adsorption of CO is an important step in the oxidation of glycerol. The adsorption of CO on the surface of the catalyst should not be too high as it can produce catalyst poisoning. If poisoning happens, the active site for the adsorption of other molecules cannot be carried out. But if adsorption is weak, the oxidation process will not be completed. The adsorption energy of CO indicates that the use of the Au catalyst model has resulted in weak adsorption. The value is 1.01 eV is weak compared to PdAu, which produces 0.61 eV in adsorption of CO. This also means that long-term endurance or durability tests using Au will be lower compared to PdAu.

## Conclusion

The catalyst of PdAu has been synthesized for oxidation reaction in Direct Glycerol Fuel Cell. The PdAu is supported on the CNF surface. The FESEM and TEM image has shown the nanoparticle of PdAu supported on CNF. The particle size of PdAu synthesized in this paper is 4 nm to 6 nm, while the CNF has a diameter size of 80 nm to 130 nm. XRD analysis has shown that PdAu is successfully allocated when peaks are shifted compared to Pd/CNF and Au/CNF. In CV analysis, PdAu/CNF has produced an oxidation peak and current density at -0.9 V vs. SCE and 70 mA/cm$^2$, respectively. From a theoretical point of view, the PdAu catalyst model has been tested for glycerol and adsorbate adsorption, where the Au catalyst model is used as a reference. Each mechanism of glycerol dissociation step during glycerol oxidation, different atomic active sites are required in PdAu. For example, for glycerol adsorption, Au atom as an active site while for *$C_3H_7O_3$ requires Pd atom and Au atom as an active site. The Au catalyst model shows better adsorption as Au/CNF has a slightly more negative oxidation peak than PdAu. Nevertheless, the Au catalyst showed less durability compared to PdAu.

## Acknowledgements

## References

Abdullah, N., Kamarudin, S.K., Shyuan, L.K. & Karim, N.A. 2017. Fabrication and characterization of new composite Ti$_{O2}$ carbon nanofiber anodic catalyst support for direct methanol fuel cell via electrospinning method. *Nanoscale Research Letters* 12(1): 613.

Alias, M.S., Kamarudin, S.K., Zainoodin, A.M. & Masdar, M.S. 2020. Active direct methanol fuel cell: An overview. *International Journal of Hydrogen Energy* 45(38): 19620-19641.

Araujo, H.R., Zanata, C.R., Teixeira-Neto, E., de Lima, R.B., Batista, B.C., Giz, M.J. & Camara, G.A. 2019. How the adsorption of Sn on Pt (100) preferentially oriented nanoparticles affects the pathways of glycerol electro-oxidation. *Electrochimica Acta* 297: 61-69.

Brueckner, T.M., Wheeler, E., Chen, B., El Sawy, E.N. & Pickup, P.G. 2019. Screening of catalysts for the electrochemical oxidation of organic fuels in a multi-anode proton exchange membrane cell. *Journal of The Electrochemical Society* 166(13): F942-F948.

Cui, X., Li, Y., Zhao, M., Xu, Y., Chen, L., Yang, S. & Wang, Y. 2019. Facile growth of ultra-small Pd nanoparticles on zeolite-templated mesocellular graphene foam for enhanced alcohol electro-oxidation. *Nano Research* 12(2): 351-356.

Day, C. & Day, G. 2017. Climate change, fossil fuel prices and depletion: The rationale for a falling export tax. *Economic Modelling* 63: 153-160.

Gao, F., Zhang, Y., Song, P., Wang, J., Yan, B., Sun, Q., Li, L., Zhu, X. & Du, Y. 2019. Shape-control of one-dimensional PtNi nanostructures as efficient electrocatalysts for alcohol electro-oxidation. *Nanoscale* 11(11): 4831-4836.

Ghosh, S., Bysakh, S. & Basu, R.N. 2019. Bimetallic Pd96Fe4 nanodendrites embedded in graphitic carbon nanosheets as highly efficient anode electrocatalysts. *Nanoscale Advances* 1(10): 3929-3940.

Houache, M.S., Hughes, K., Ahmed, A., Safari, R., Liu, H., Botton, G.A. & Baranova, E.A. 2019. Electrochemical valorization of glycerol on Ni-rich bimetallic NiPd nanoparticles: Insight into product selectivity using *in situ* polarization modulation infrared-reflection absorption spectroscopy. *ACS Sustainable Chemistry & Engineering* 7(17): 14425-14434.

Karim, N.A. & Kamarudin, S.K. 2017. Novel heat-treated cobalt phthalocyanine/carbon-tungsten oxide nanowires (CoPc/C-W18O49) cathode catalyst for direct methanol fuel cell. *Journal of Electroanalytical Chemistry* 803: 19-29.

Karim, N.A., Kamarudin, S.K. & Loh, K.S. 2017. Performance of a novel non-platinum cathode catalyst for direct methanol fuel cells. *Energy Conversion and Management* 145: 293-307.

Martins, C.A., Ibrahim, O.A., Pei, P. & Kjeang, E. 2019. *In situ* decoration of metallic catalysts in flow-through electrodes: Application of Fe/Pt/C for glycerol oxidation in a microfluidic fuel cell. *Electrochimica Acta* 305: 47-55.

Mori, D. & Hirose, K. 2009. Recent challenges of hydrogen storage technologies for fuel cell vehicles. *International Journal of Hydrogen Energy* 34(10): 4569-4574.

Nascimento, A.P. & Linares, J.J. 2014. Performance of a direct glycerol fuel cell using KOH doped polybenzimidazole as electrolyte. *Journal of the Brazilian Chemical Society* 25(3): 509-516.

Ning, X., Zhou, X., Luo, J., Ma, L., Xu, X. & Zhan, L. 2019. Glycerol and formic acid electro-oxidation over Pt on S-doped carbon nanotubes: Effect of carbon support and synthesis method on the metal-support interaction. *Electrochimica Acta* 319: 129-137.

Sun, Q., Gao, F., Zhang, Y., Wang, C., Zhu, X. & Du, Y. 2019. Ultrathin one-dimensional platinum-cobalt nanowires as efficient catalysts for the glycerol oxidation reaction. *Journal of Colloid and Interface Science* 556: 441-448.

Tam, B., Duca, M., Wang, A., Fan, M., Garbarino, S. & Guay, D. 2019. Promotion of glycerol oxidation by selective Ru decoration of (100) domains at nanostructured Pt electrodes. *ChemElectroChem* 6(6): 1784-1793.

Wang, C., Song, P., Gao, F., Song, T., Zhang, Y., Chen, C., Li, L., Jin, L. & Du, Y. 2019. Precise synthesis of monodisperse PdAg nanoparticles for size-dependent electrocatalytic oxidation reactions. *Journal of Colloid and Interface Science* 544: 284-292.

Wang, J., Wang, H. & Fan, Y. 2018. Techno-economic challenges of fuel cell commercialization. *Engineering* 4(3): 352-360.

Wang, W., Wang, Z., Wang, J., Zhong, C.J. & Liu, C.J. 2017. Highly active and stable Pt-Pd alloy catalysts synthesized by

room-temperature electron reduction for oxygen reduction reaction. *Advanced Science* 4(4): 1600486.

Yahya, N., Kamarudin, S.K., Karim, N.A., Masdar, M.S. & Loh, K.S. 2017. Enhanced performance of a novel anodic PdAu/VGCNF catalyst for electro-oxidation in a glycerol fuel cell. *Nanoscale Research Letters* 12 (1): 605.

Zakaria, K., McKay, M., Thimmappa, R., Hasan, M., Mamlouk, M. & Scott, K. 2019. Direct glycerol fuel cells: Comparison with direct methanol and ethanol fuel cells. *ChemElectroChem* 6(9): 2578-2585.

Zhang, Y., Gao, F., Song, P., Wang, J., Song, T., Wang, C., Chen, C., Jin, L., Li, L., Zhu, X. & Du, Y. 2019. Superior liquid fuel oxidation electrocatalysis enabled by novel bimetallic PtNi nanorods. *Journal of Power Sources* 425: 179-185.

Zhang, Z.C., Lerner, B., Lei, G.D. & Sachtler, W.M.H. 1993. Hydrocarbon-induced agglomeration of Pd particles in Pd/HZSM-5. *Journal of Catalysis* 140(2): 481-496.

Zhou, Y., Shen, Y., Xi, J. & Luo, X. 2019. Selective electro-oxidation of glycerol to dihydroxyacetone by PtAg skeletons. *ACS Applied Materials & Interfaces* 11(32): 28953-28959.

Nabila A. Karim*, Muhammad Syafiq & Siti Kartom Kamarudin
Fuel Cell Institute
Universiti Kebangsaan Malaysia
43600 UKM Bangi, Selangor Darul Ehsan
Malaysia

Norilhamiah Yahya
Malaysian Institute of Chemical and Bioengineering Technology
Universiti Kuala Lumpur
78000 Alor Gajah, Melaka
Malaysia

*Corresponding author; email: nabila.akarim@ukm.edu.my